Spontaneous seizure and memory loss in mice expressing an epileptic encephalopathy variant in the calmodulin-binding domain of $K_v7.2$

Eung Chang Kim[a], Jiaren Zhang[a], Andy Y. Tang[a], Eric C. Bolton[a], Justin S. Rhodes[b,c,d], Catherine A. Christian-Hinman[a,b,d], and Hee Jung Chung[a,b,d,1]

[a]Department of Molecular and Integrative Physiology, University of Illinois at Urbana–Champaign, Urbana, IL 61801; [b]Beckman Institute for Advanced Science and Technology, University of Illinois at Urbana–Champaign, Urbana, IL 61801; [c]Department of Psychology, University of Illinois at Urbana–Champaign, Urbana, IL 61801; and [d]Neuroscience Program, University of Illinois at Urbana–Champaign, Urbana, IL 61801

Edited by Lily Jan, HHMI and Department of Physiology and Biochemistry, University of California, San Francisco, CA; received October 12, 2020; accepted November 7, 2021

Epileptic encephalopathy (EE) is characterized by seizures that respond poorly to antiseizure drugs, psychomotor delay, and cognitive and behavioral impairments. One of the frequently mutated genes in EE is *KCNQ2*, which encodes the $K_v7.2$ subunit of voltage-gated K_v7 potassium channels. K_v7 channels composed of $K_v7.2$ and $K_v7.3$ are enriched at the axonal surface, where they potently suppress neuronal excitability. Previously, we reported that the de novo dominant EE mutation M546V in human $K_v7.2$ blocks calmodulin binding to $K_v7.2$ and axonal surface expression of K_v7 channels via their intracellular retention. However, whether these pathogenic mechanisms underlie epileptic seizures and behavioral comorbidities remains unknown. Here, we report conditional transgenic c*Kcnq2*$^{+/M547V}$ mice, in which expression of mouse $K_v7.2$-M547V (equivalent to human $K_v7.2$-M546V) is induced in forebrain excitatory pyramidal neurons and astrocytes. These mice display early mortality, spontaneous seizures, enhanced seizure susceptibility, memory impairment, and repetitive behaviors. Furthermore, hippocampal pathology shows widespread neurodegeneration and reactive astrocytes. This study demonstrates that the impairment in axonal surface expression of K_v7 channels is associated with epileptic seizures, cognitive and behavioral deficits, and neuronal loss in *KCNQ2*-related EE.

KCNQ2 | seizures | epilepsy

Epileptic encephalopathies (EEs) are a collection of heterogeneous disorders in which early-onset severe seizures contribute to developmental delay and progressive cognitive and behavioral impairments (1). Current treatments for EEs have limited efficacy in alleviating seizures and comorbidities (2), posing an urgent need to understand the etiology of EEs and find new therapeutic targets. Recent discoveries of epilepsy-related genes in multiple laboratories and through the large Epi4K, EpiPM, and EuroEPINOMICS-RES consortia have identified a diverse array of proteins that may contribute to epileptogenesis (3–5). Among them, dominant variants associated with benign familial neonatal epilepsy (BFNE) and EE have been found in *KCNQ2* and *KCNQ3* genes, which encode the $K_v7.2$ and $K_v7.3$ subunits of voltage-gated potassium (K^+) channel subfamily Q (K_v7) (https://www.rikee.org; ClinVar Database, National Center for Biotechnology Information [NCBI]).

Neuronal K_v7 channels are mostly heterotetrameric channels of $K_v7.2$ and $K_v7.3$ subunits (6), which have overlapping distribution in the central nervous system including the cerebral cortex and hippocampus (7). In neurons, they are preferentially localized to the axonal plasma membrane with the highest concentration at the axonal initial segment (AIS) (7, 8), where the action potential (AP) initiates (9). They give rise to the slowly activating and noninactivating outward K^+ current termed M current (I_M) (6). Because they open at subthreshold potentials (6), I_M potently suppresses AP firing (6, 10, 11), underscoring their critical roles in reducing neuronal excitability. By contrast, activation of G_q-coupled receptors, including muscarinic acetylcholine receptors, inhibits I_M by depleting the lipid cofactor PIP_2, resulting in enhanced AP firing (12).

To date, 193 dominant variants in *KCNQ2* and 2 variants in *KCNQ3* have been identified in patients with EE (https://www.rikee.org; ClinVar Database, NCBI). EE variants are clustered at the functional domains of $K_v7.2$ important for voltage-dependent opening of K_v7 channels (13) and typically decrease the function of heterotetrameric channels by 20 to 75% (13–17). EE variants are also enriched at helices A and B in the intracellular C-terminal tail of $K_v7.2$ (13, 14, 16), which mediate calmodulin (CaM) binding critical for axonal enrichment of K_v7 channels (18). Among these variants, a mutation of methionine at amino acid position 546 to valine (M546V) was found in a male patient who displayed drug-resistant neonatal tonic-clonic seizures and later developed profound intellectual and language disability, spasticity, and autistic behavior (15). While this mutation in helix B abolishes current expression of homomeric but not heteromeric channels in heterologous cells (14, 17), it severely reduces CaM binding and axonal surface expression of heteromeric channels in cultured hippocampal neurons (14). This mutation also induces

Significance

Epileptic encephalopathy (EE) is a devastating neurologic disorder characterized by early-onset seizures with severe cognitive and psychomotor impairments. EE is associated with dominant mutations in the KCNQ2 gene which encodes the $K_v7.2$ subunit of K_v7 potassium channels. Previously, we reported that multiple EE mutations in the intracellular calmodulin-binding domain of $K_v7.2$ decreased surface expression of axonal K_v7 channels critical for suppressing neuronal excitability. Here, we generated conditional knockin mice carrying one of these mutations, M547V. These mice displayed spontaneous seizures, cognitive impairment, neurodegeneration, and reactive astrogliosis, implicating abnormal K_v7 surface expression as a key etiology of *KCNQ2*-associated EE.

Author contributions: E.C.K., J.Z., and H.J.C. designed research; E.C.K., J.Z., E.C.B., and H.J.C. performed research; A.Y.T., E.C.B., J.S.R., C.A.C.-H., and H.J.C. contributed new reagents/analytic tools; E.C.K., J.Z., A.Y.T., E.C.B., and H.J.C. analyzed data; and E.C.K., J.Z., E.C.B., and H.J.C. wrote the paper.

The authors declare no competing interest.

This article is a PNAS Direct Submission.

[1]To whom correspondence may be addressed. Email: chunghj@life.illinois.edu.

This article contains supporting information online at http://www.pnas.org/lookup/suppl/doi:10.1073/pnas.2021265118/-/DCSupplemental.

Published December 15, 2021.

ubiquitination and proteasomal degradation of $K_v7.2$, whereas the presence of $K_v7.3$ blocks this degradation and accumulates ubiquitinated $K_v7.2$ (14). However, whether these pathogenic mechanisms underlie epileptic seizures and behavioral deficits in EE remains unknown.

In this study, we investigated the contribution of the EE variant M546V by generating conditional transgenic mice in which heterozygous expression of mouse $K_v7.2$-M547V was induced in forebrain excitatory pyramidal neurons. M546 in the human $K_v7.2$ is conserved in the mouse $K_v7.2$ at amino acid position 547. These mice showed widespread neurodegeneration and reactive astrogliosis in the hippocampus and cortex, and displayed spontaneous seizures and cognitive deficit, providing a causal link between M546V-mediated disruption of axonal surface expression of K_v7 channels and *KCNQ2*-associated EE.

Results

***cKcnq2*$^{+/M547V}$ Mice Have Reduced Viability.** We used CRISPR-Cas–mediated genome engineering to generate a conditional knockin (KI) mouse line in the C57BL/6J background for the murine *Kcnq2* gene (GenBank accession no. NM_010611.3) containing the mutation M547V, which corresponds to M546V in the long isoform of human $K_v7.2$ (GenBank accession no. NM_172107.4: c.1636A>G) and M518V in the short isoform (GenBank accession no. Y15065.1) and is located at the CaM contact site in helix B (Fig. 1*A*) (14, 17). This *Kcnq2*-M547V$^{fl/fl}$ line contains a floxed-STOP cassette upstream of *Kcnq2*-M547V-ires-EGFP at the Gt(ROSA)26Sor locus (Fig. 1*B*). Upon removal of an upstream floxed-STOP cassette by Cre recombinase, this line expresses both *Kcnq2*-M547V and enhanced green fluorescent protein (EGFP) (Fig. 1*B* and *SI Appendix*, Fig. S1).

We chose this strategy because expression of this human EE mutant $K_v7.2$ causes cell death in HEK293T cells and hippocampal neuronal culture (14), and thus we anticipated high mortality of the KI progeny produced by homologous recombination of *Kcnq2*-M547V into the genomic *Kcnq2* sequence. This strategy also allows us to express the *Kcnq2*-M547V-ires-EGFP transgene in heterozygous *Kcnq2* knockout (KO) mice to induce heterozygous KI of *Kcnq2*-M547V (designated as *cKcnq2*$^{+/M547V}$) or in wild-type (WT) mice in case heterozygous KI leads to high mortality (designated as *cKcnq2*$^{pyr\text{-}M547V}$) (Fig. 1*C*).

We crossed *Kcnq2*-M547V$^{fl/fl}$ mice to heterozygous *Kcnq2* KO mice (*Kcnq2*$^{tm1Dgen/+}$) (19) and Emx1-ires-cre (Emx1$^{cre/cre}$) mice, which express Cre during neurogenesis in excitatory pyramidal neurons in the hippocampus and cortex (20), where endogenous $K_v7.2$ and $K_v7.3$ are highly expressed (7). The resulting progenies are *cKcnq2*$^{+/M547V}$ (*Kcnq2*-M547V$^{fl/+}$:*Kcnq2*$^{tm1Dgen/+}$:Emx1$^{cre/+}$), *cKcnq2*$^{pyr\text{-}M547V}$ (*Kcnq2*-M547V$^{fl/+}$:Emx1$^{cre/+}$), *Kcnq2*$^{+/-}$ (*Kcnq2*$^{tm1Dgen/+}$), and the WT control mice (*Kcnq2*$^{+/+}$, *Kcnq2*-M547V$^{fl/+}$, and Emx1$^{cre/+}$) (Fig. 1*C*). Their genotypes were confirmed by PCR of tail genomic DNA (Fig. 1*D*). Although a single copy of *Kcnq2*-M547V-ires-EGFP is expected to express in *cKcnq2*$^{+/M547V}$ mice, *Kcnq2* messenger RNA level in *cKcnq2*$^{+/M547V}$ mice was 1.94-fold higher than that in control Emx1$^{cre/+}$ mice (*SI Appendix*, Fig. S2), most likely due to the CAG promoter–driven expression of the transgene (Fig. 1*B*). Compared with control mice, the protein level of $K_v7.2$ in the hippocampi of *cKcnq2*$^{+/M547V}$ mice was twofold higher at postnatal day (P) 1, 45% lower at P30, and comparable at P60 and P120 (Fig. 1*E* and *SI Appendix*, Figs. S3, S4, and S5*A*).

Kaplan–Meier survival plots indicate that ∼40% of *cKcnq2*$^{+/M547V}$ mice died by P10 (Fig. 1*F*) despite the expected Mendelian inheritance at birth (*SI Appendix*, Fig. S5*C*). By contrast, *Kcnq2*$^{+/-}$ and control mice had minimal death (Fig. 1*F*). By P21, *cKcnq2*$^{+/M547V}$ mice also displayed abnormal behaviors including continuous jumping and digging in their home cage (Movies S1 and S2). Some showed motionless and rigid postures (Movie S3). Curiously, the high mortality of *cKcnq2*$^{+/M547V}$ mice was not observed from P21 (Fig. 1*G*). There were no obvious differences in gross brain appearance or size between genotypes at P30 and P120 (*SI Appendix*, Fig. S6 *A* and *B*). The surviving *cKcnq2*$^{+/M547V}$ males weighed less than control males at P120, but this genotype difference was not observed in females (*SI Appendix*, Fig. S6*C*).

***cKcnq2*$^{+/M547V}$ Mice Display Spontaneous Seizures and Extreme Seizure Sensitivity to Kainic Acid.** The patient with the de novo M546V mutation displayed drug-resistant neonatal tonic-clonic seizures (15). To test if spontaneous seizures occur in *cKcnq2*$^{+/M547V}$ mice, we performed simultaneous video monitoring of behavioral seizures and electroencephalogram (EEG) recording at P60 to P85 (Fig. 2 *A*–*C*). All *cKcnq2*$^{+/M547V}$ males displayed recurrent spontaneous behavioral seizures followed by death during recovery from electrode implantation surgery, precluding EEG recordings. Of six *cKcnq2*$^{+/M547V}$ females, three survived for EEG recording. Two mice demonstrated spontaneous electrographic seizures that coincided with stage 4 and 7 seizures (Fig. 2 *B* and *C* and Movies S4 and S5). By contrast, *Kcnq2*$^{+/+}$ females did not show electrographic and behavioral seizures (Fig. 2*A*).

Although *Kcnq2*$^{+/-}$ mice do not have spontaneous seizures (19, 21), they display enhanced sensitivity to seizures induced by pentylenetetrazole (21) and kainic acid (KA) (22). To compare seizure propensity of *cKcnq2*$^{+/M547V}$ mice with that of *Kcnq2*$^{+/-}$ mice, the mice (P120 to P180) received systemic injection of KA to induce seizures that arise from the hippocampus (23). A lower dose of KA (15 mg/kg, intraperitoneal [i.p.]) was used to reduce mortality (22). Control mice displayed only transient stage 2 seizures, whereas *cKcnq2*$^{+/M547V}$ mice showed stage 8 seizures by 40 min post-KA injection (Fig. 2*D*) and displayed a significantly higher cumulative seizure score and shorter latency to stage 4 seizure and death than control mice regardless of sex (Fig. 2 *E*–*G* and *SI Appendix*, Table S1). *Kcnq2*$^{+/-}$ males and females reached stage 4 and 6 seizures, respectively, by 40 min post-KA injection (Fig. 2*D*) and displayed a lower cumulative seizure score than *cKcnq2*$^{+/M547V}$ mice (Fig. 2*E*). These results indicate that *cKcnq2*$^{+/M547V}$ mice had significantly higher seizure susceptibility than *Kcnq2*$^{+/-}$ mice.

***cKcnq2*$^{+/M547V}$ Mice Display Cognitive Deficits and Abnormal Behaviors.** The patient with the M546V mutation had profound intellectual disability, spasticity, and autistic behavior (15). To test if these comorbidities occur in *cKcnq2*$^{+/M547V}$ mice, we performed six behavioral tests at P120 during the dark phase (Fig. 3*A*). There was no gross abnormality in motor coordination of *cKcnq2*$^{+/M547V}$ mice as indicated by their similar latency to fall from the rotarod compared with control mice (Fig. 3*B* and *SI Appendix*, Table S2). In the open-field test, *cKcnq2*$^{+/M547V}$ males traveled a longer distance in the entire open-field arena than control males (Fig. 3*C* and *SI Appendix*, Table S2), indicative of hyperactivity. Both *cKcnq2*$^{+/M547V}$ males and females displayed higher numbers of entries into the center of the arena, spent more time, and traveled a longer distance within the center than control mice (Fig. 3*C* and *SI Appendix*, Table S2), suggesting enhanced exploratory behavior or reduced anxiety-like behavior.

To test if *cKcnq2*$^{+/M547V}$ mice display cognitive deficits, we performed the object-location task (OLT) and novel object–recognition task (NORT). The OLT evaluates hippocampus-dependent spatial memory, whereas the NORT tests nonspatial memory of object identity (24). During the OLT, control mice spent significantly more time with the moved object, whereas

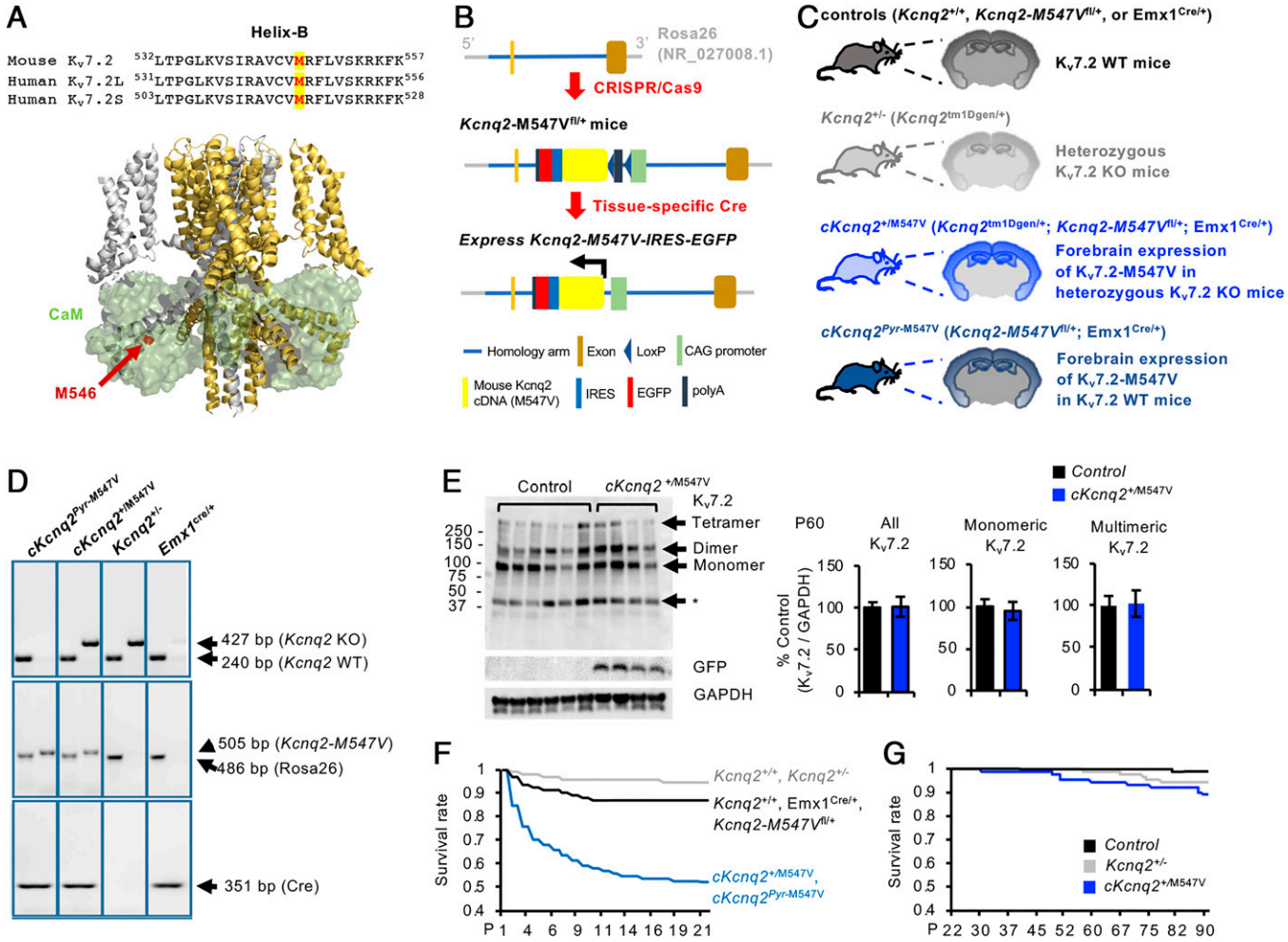

Fig. 1. Conditional *cKcnq2*$^{+/M547V}$ mice display increased early mortality. (*A*, *Top*) Sequence alignment of helix B in which M547 in the mouse $K_v7.2$ (NP_034741.2), M546V in the human $K_v7.2$ long isoform ($K_v7.2$ L, NP_742105.1), and M518V in the human $K_v7.2$ short isoform ($K_v7.2$ S, NP_004509.2) are labeled in red and highlighted in yellow. (*A*, *Bottom*) The Cα atom of M546V is highlighted in red in one subunit of the cryo-EM structure of human $K_v7.2$ (ribbons) in complex with four CaM subunits (transparent green surfaces). (*B*) Schematic diagram (not to scale) showing the targeting strategy for conditional expression of $K_v7.2$-M547V in mice. In *Kcnq2*-M547V$^{fl/fl}$ mice, the *CAG-LoxP-Stop-LoxP* mouse *Kcnq2-M547V cDNA (NM_010611.3)-IRES-EGFP-polyA* cassette was cloned into intron 1 of the *ROSA26* allele by CRISPR-Cas–mediated genome engineering. Upon removal of an upstream floxed-STOP cassette by Cre recombinase, this line expresses the *Kcnq2*-M547V and EGFP transgene. (*C*) Schematic representation of coronal brain sections of the progenies that result from breeding conditional *Kcnq2*-M547V$^{fl/fl}$ mice, heterozygous KO *Kcnq2*$^{+/-}$ mice (*Kcnq2*$^{tm1Dgen/+}$), and the Emx1-ires-cre mice (Emx1$^{cre/cre}$) that express Cre recombinase in forebrain excitatory pyramidal neurons from embryonic day 10.5. The *cKcnq2*$^{+/M547V}$ mice (*Kcnq2*-M547V$^{fl/+}$: *Kcnq2*$^{tm1Dgen/+}$: Emx1^{cre}/$^{+}$) express *Kcnq2*-M547V-ires-EGFP in the forebrain excitatory pyramidal neurons of *Kcnq2*$^{+/-}$ mice, whereas *cKcnq2*$^{pyr-M547V}$ mice express this transgene in WT *Kcnq2*$^{+/+}$ mice. (*D*) Representative example of a genotyping PCR using mouse tail genomic DNA as template. (*E*) Western blots of $K_v7.2$ and glyceraldehyde 3-phosphate dehydrogenase (GAPDH) in the hippocampal homogenates (soluble S1 fractions) of control mice (Emx1$^{cre/+}$) and *cKcnq2*$^{+/M547V}$ mice at P60. The identities of bands (asterisk) below 50 kDa are unclear. The *cKcnq2*$^{+/M547V}$ mice displayed similar hippocampal protein expression of $K_v7.2$ compared with control mice. The total number of mice used for quantification at P60: control (n = 6 including 3 males and 3 females) and *cKcnq2*$^{+/M547V}$ (n = 4 including 2 males and 2 females). Data are shown as mean ± SEM. Two-tailed Student's t test was performed. Western blot quantification of $K_v7.2$ at P30 and P120 is shown in *SI Appendix*, Figs. S3 and S4. (*F*) Kaplan–Meier survival plots for all mice used in this study from P0 to P21. Out of 407 *cKcnq2*$^{pyr-M547V}$ and *cKcnq2*$^{+/M547V}$ mice, only 213 survived, including 128 *cKcnq2*$^{pyr-M547V}$ mice and 83 *cKcnq2*$^{+/M547V}$ mice. By contrast, 356 out of 409 control mice survived. Out of 282 *Kcnq2*$^{+/+}$ and *Kcnq2*$^{+/-}$ mice, 267 survived, including 106 *Kcnq2*$^{+/-}$ mice and 161 *Kcnq2*$^{+/+}$ mice. (*G*) Kaplan–Meier survival plots for control (n = 356), *Kcnq2*$^{+/-}$ (n = 106), and *cKcnq2*$^{+/M547V}$ (n = 83) from P22 to P90.

cKcnq2$^{+/M547V}$ mice did not (Fig. 3*D* and *SI Appendix*, Table S2). During the NORT, control but not *cKcnq2*$^{+/M547V}$ mice spent significantly more time exploring the novel object (Fig. 3*D* and *SI Appendix*, Table S2). These results indicate that *cKcnq2*$^{+/M547V}$ mice showed impaired object-recognition memory and hippocampus-dependent spatial memory.

We next tested if *cKcnq2*$^{+/M547V}$ mice display autism-like behaviors including social avoidance and repetitive behaviors. In the three-chamber social interaction test (25), both genotypes spent significantly more time on the side of the chamber containing a novel social target mouse as compared with the empty side (Fig. 3*E* and *SI Appendix*, Table S3). While there were no genotype differences in males for sniffing duration and frequency, *cKcnq2*$^{+/M547V}$ females sniffed the novel mouse for a shorter duration and frequency than control females (Fig. 3*E* and *SI Appendix*, Table S3), indicative of reduced sociability. When another novel mouse was placed in the empty side (*SI Appendix*, Fig. S7), both genotypes spent more time sniffing the new mouse than the familiar mouse (*SI Appendix*, Fig. S7 and Table S4), suggesting that social preference of the novel mouse is similar between *cKcnq2*$^{+/M547V}$ and control mice.

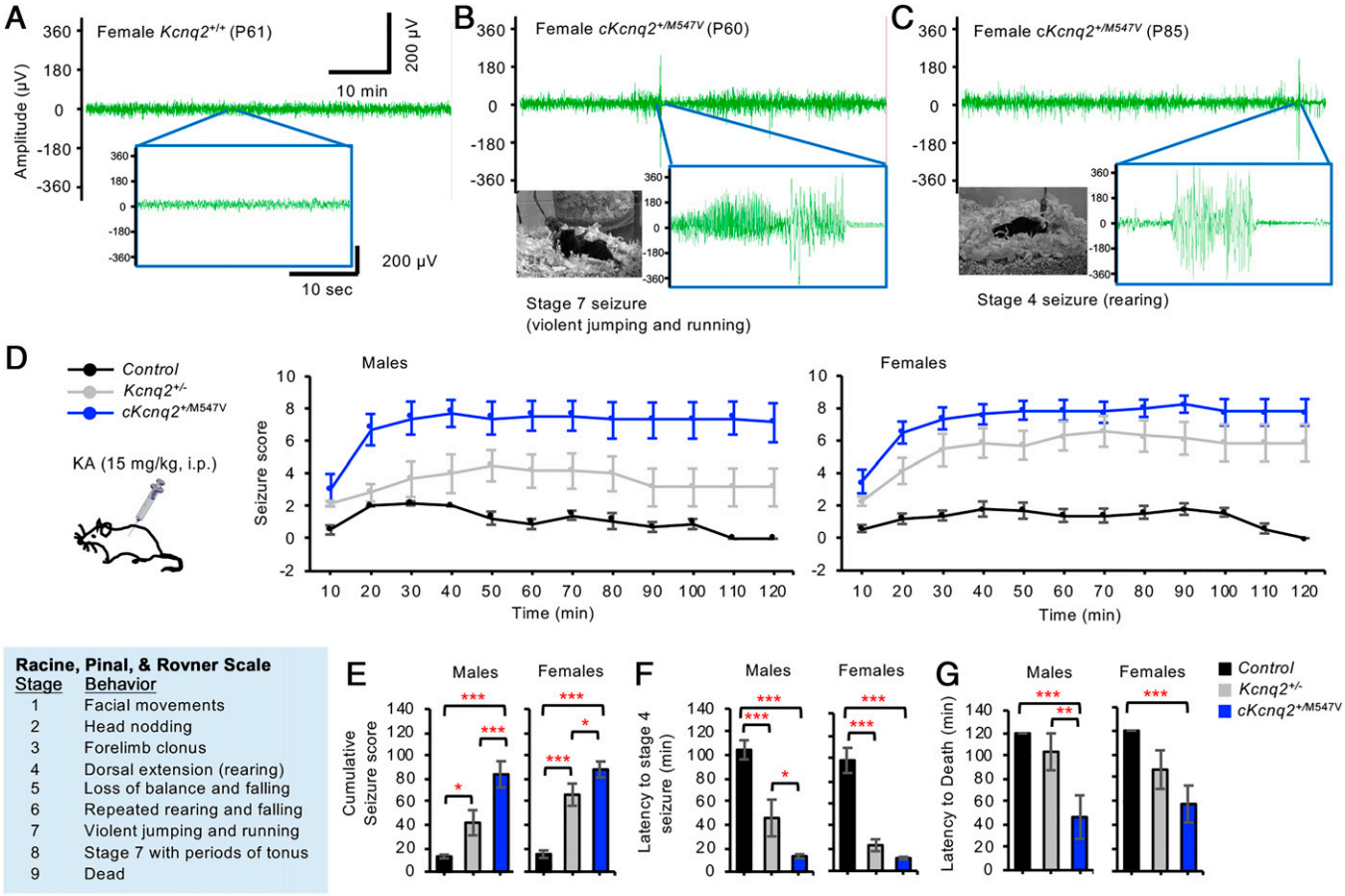

Fig. 2. Conditional *cKcnq2*$^{M547V/+}$ mice showed spontaneous seizures and extreme seizure sensitivity to KA. (*A*–*C*) The control (*Kcnq2*$^{+/+}$) and *cKcnq2*$^{+/M547V}$ mice were subjected to a simultaneous video and EEG monitoring. (*A*) A female control *Kcnq2*$^{+/+}$ mouse at P61 showed no electrographic or behavioral seizures. The baseline activity showed the mean peak amplitude of 28.0 ± 0.4 μV and a frequency of 0.26 ± 0.10 Hz. (*B*) A *cKcnq2*$^{+/M547V}$ female mouse at P60 displayed spontaneous electrographic seizures that coincided with stage 7 behavior seizures. The mean peak amplitudes were 121.7 ± 2.2 μV during stage 7 seizure and 28.6 ± 1.10 μV during the baseline. (*C*) Another *cKcnq2*$^{+/M547V}$ female mouse at P85 displayed spontaneous electrographic seizures that coincided with stage 4 behavioral seizures with the mean peak amplitude of 103.1 ± 4.9 μV. Interestingly, the baseline activity of this mouse showed a larger peak amplitude (31.5 ± 0.5 μV, $P < 0.05$) and a higher frequency (2.73 ± 0.36 Hz, $P < 0.005$) than the *Kcnq2*$^{+/+}$ female in *B*. The behavioral seizures of the *cKcnq2*$^{+/M547V}$ female mice in *B* and *C* are shown in Movies S4 and S5. (*D*–*G*) The control (*Kcnq2*$^{+/+}$, *Kcnq2*-M547V$^{fl/+}$, Emx1$^{cre/+}$), *Kcnq2*$^{+/-}$, and *cKcnq2*$^{+/M547V}$ mice (P120 to P180) were injected with a low dose of KA (15 mg/kg, i.p.) and their behavioral seizures were rated with a modified Racine, Pinal, and Rovner scale at each 10-min interval. (*D* and *E*) Average seizure scores (*D*) and cumulative seizure scores (*E*) per mouse over the first 2 h after KA injection. (*F*) Latency to stage 4 seizure. (*G*) Latency to death. Data are shown as mean ± SEM. The number of male mice used: control ($n = 10$), *Kcnq2*$^{+/-}$ ($n = 7$), and *cKcnq2*$^{+/M547V}$ ($n = 8$). The number of female mice used: control ($n = 10$), *Kcnq2*$^{+/-}$ ($n = 8$), and *cKcnq2*$^{+/M547V}$ ($n = 7$). Post hoc Tukey test results are shown here (*$P < 0.05$, **$P < 0.01$, ***$P < 0.005$). *SI Appendix*, Table S1 shows two-way ANOVA test results for control and with genotype as one factor and sex as the other.

Compared with control mice, *cKcnq2*$^{+/M547V}$ mice displayed a longer duration of a grooming event and shorter latency of grooming (Fig. 3*F* and *SI Appendix*, Table S2), indicating increased repetitive behaviors (26). In addition, sex differences were observed for latency of grooming (*SI Appendix*, Table S2). In a marble-burying test (27), *cKcnq2*$^{+/M547V}$ males buried four times as many marbles as control males, but this genotype difference was not observed in females (Fig. 3*G* and *SI Appendix*, Table S2), indicating that *cKcnq2*$^{+/M547V}$ males displayed enhanced repetitive and compulsive-like behaviors.

***cKcnq2*$^{+/M547V}$ Mice Display Neurodegeneration and Reactive Astrogliosis.** To understand the pathologic basis for spontaneous seizures and behavioral deficits of *cKcnq2*$^{+/M547V}$ mice, we next performed immunostaining with verified anti-K_v7.2 antibodies (*SI Appendix*, Fig. S8). The hippocampi and cortices of *cKcnq2*$^{+/M547V}$ mice showed GFP expression at P30, P60, and P120, whereas those of control mice did not (*SI Appendix*, Fig. S1), indicating Cre-dependent expression of the *Kcnq2*-M547V-ires-EGFP transgene in forebrain pyramidal neurons (Fig. 1*B*). In the hippocampi of control mice at P120, we observed strong immunolabeling of K_v7.2 in the apical dendrites of CA1 neurons (Fig. 4*A*). In *cKcnq2*$^{+/M547V}$ mice, K_v7.2 immunostaining was jagged in the stratum radiatum but was overall similar to control mice throughout the hippocampi (Fig. 4*A* and *SI Appendix*, Fig. S9 *A*–*C*). Interestingly, K_v7.2 and ankyrin-G expression at the AIS was weaker in the cortical pyramidal neurons of *cKcnq2*$^{+/M547V}$ mice compared with control mice (*SI Appendix*, Fig. S9*D*).

Surprisingly, K_v7.2 proteins were also detected as large perinuclear puncta in some glial fibrillary acidic protein (GFAP)–positive cells in *cKcnq2*$^{+/M547V}$ mice (*SI Appendix*, Fig. S12), which colocalize with GFP but not neuronal marker NeuN (*SI Appendix*, Fig. S13). Although the original study on the Emx1-cre line reports Cre expression in primary neocortical astrocyte culture but not in the cortex in vivo (20), the presence of K_v7.2 and GFP in astrocytes of *cKcnq2*$^{+/M547V}$ mice suggests unexpected Cre activity in off-target cells of the widely used Emx1-Cre strain.

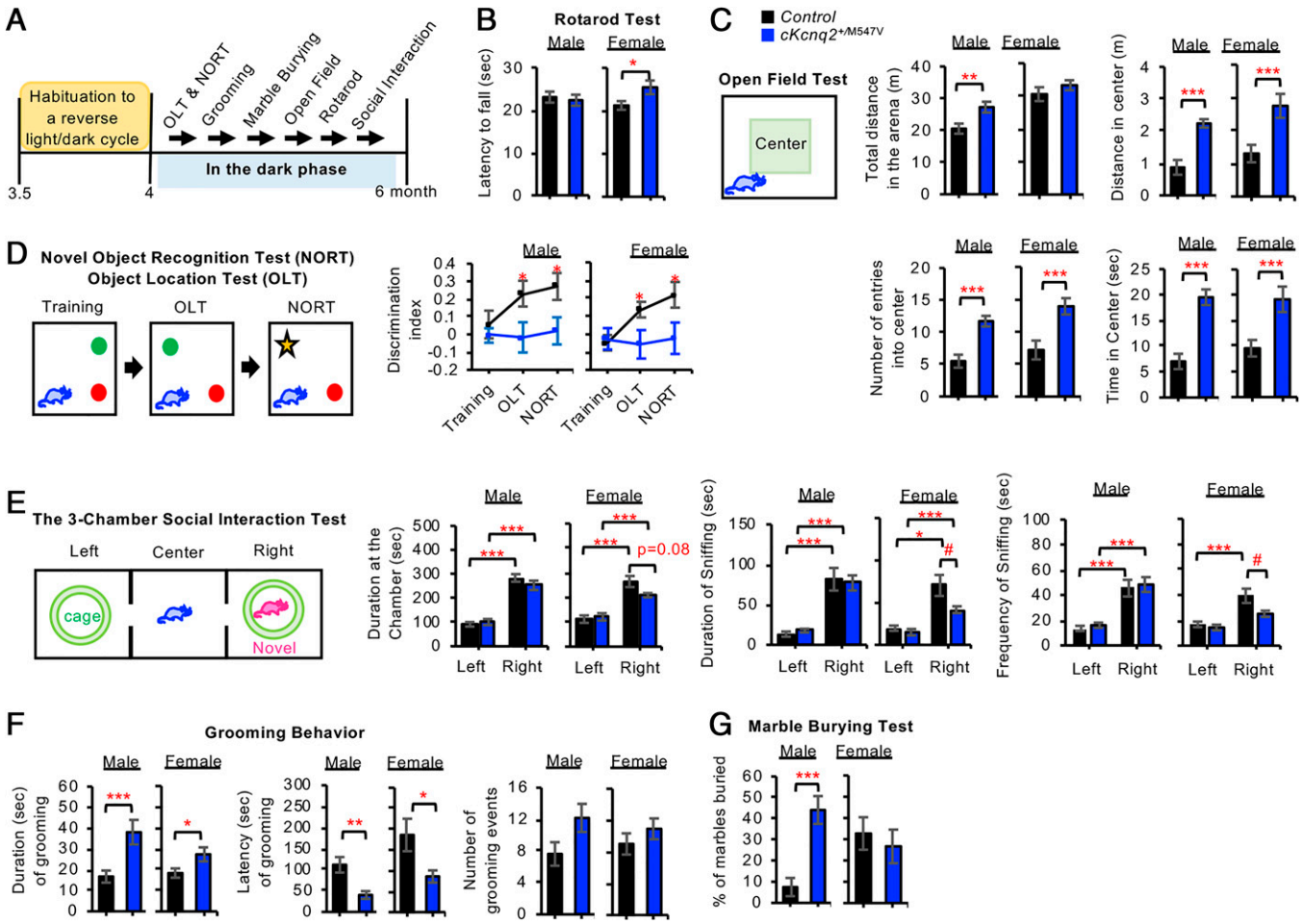

Fig. 3. Conditional *cKcnq2*$^{M547V/+}$ mice displayed reduced cognition and abnormal behaviors reminiscent of autism. (*A*) Control and *cKcnq2*$^{+/M547V}$ mice (P120) were subjected to a battery of behavioral tests in the dark phase with a test interval of >2 d. (*B*) Latency to fall in the rotarod test. (*C*) The open-field test was performed to record the total distance traveled throughout the open-field arena, entries into the center zone, duration spent within the center zone, and distance traveled within the center zone. (*D*) The time spent exploring both novel and familiar objects was recorded in the OLT and NORT to calculate the discrimination index as $(Time_{novel} - Time_{familiar})/(Time_{novel} + Time_{familiar})$. (*E*) In the "sociability" examination of the three-chamber social interaction test, a novel stranger mouse (age-matched C57BL/6J) was placed inside the wire cage of the right chamber, and the test mouse was introduced into the center chamber and allowed to explore for 10 min. The time spent in the left and right chambers, as well as the duration, latency, and frequency of sniffing behavior, was quantified. (*F*) Quantification of the grooming events in their home cages without the bedding. (*G*) Quantification of the percentage (%) of the marbles buried in the marble-burying test. Data shown represent the mean ± SEM. The number of male mice used: control (n = 8, *Kcnq2*-M547V$^{fl/+}$) and *cKcnq2*$^{+/M547V}$ (n = 11). The number of female mice used: control (n = 8, *Kcnq2*-M547V$^{fl/+}$) and *cKcnq2*$^{+/M547V}$ (n = 11). Data are shown as mean ± SEM. Two-tailed Student's t test results are shown in *B*, *C*, *F*, and *G*, whereas post hoc Tukey test results are shown in *D* and *E* ($^{\#}P < 0.05$, $^{*}P < 0.05$, $^{**}P < 0.01$, $^{***}P < 0.005$). *SI Appendix*, Table S2 shows two-way ANOVA test results for all behavioral tests except the social interaction tests with genotype as one factor and sex as the other. *SI Appendix*, Table S3 shows two-way ANOVA test results for the social interaction tests per sex with chamber as one factor and genotype as the other.

We have previously shown that the analogous M546V mutation in human $K_v7.2$ induces not only ubiquitination but also severe impairments in axonal surface expression of $K_v7.2/K_v7.3$ channels and their intracellular retention (14). Intracellular accumulation of polyubiquitinated proteins in the endoplasmic reticulum (ER) has been shown to induce cell death (28). To test if expression of $K_v7.2$-M547V induces neuronal death in vivo, brain cryosections were subjected to staining with Fluoro-Jade C, a fluorescein-derived fluorochrome which specifically binds to degenerating neurons (29). Fluoro-Jade C staining revealed a larger number of degenerating hippocampal neurons in *cKcnq2*$^{+/M547V}$ mice than in control mice in P30, P60, and P120 (Fig. 4*B* and *SI Appendix*, Fig. S14).

Reactive astrocytes mediate neuroinflammation by secreting inflammatory factors and function as phagocytes for degenerated axons and apoptotic neurons in brain injury and neurodegenerative diseases (30). Compared with control mice, *cKcnq2*$^{+/M547V}$ hippocampi showed significant age-dependent increases in the number of astrocytes and GFAP expression per astrocyte (Fig. 4 *C*–*E* and *SI Appendix*, Figs. S10–S12), indicative of the activation and significant presence of reactive astrocytes (30).

Discussion

Contribution of the Forebrain Expression of $K_v7.2$-M547V to Epileptic Seizures in Mice. Most children with BFNE and EE mutations in *KCNQ2* and *KCNQ3* have mild epileptic seizures that are remitted later in life or managed by antiseizure drugs (31). A subset of children has a more severe disease phenotype including refractory seizures (31). One such mutation is M546V, located in the CaM-binding helix B of $K_v7.2$ (15). We show that *cKcnq2*$^{+/M547V}$ mice displayed spontaneous generalized tonic-clonic seizures as early as P60 (Fig. 2 *A*–*C*) and continuous jumping and prolonged rigidity by P21 (Movies S1–S3).

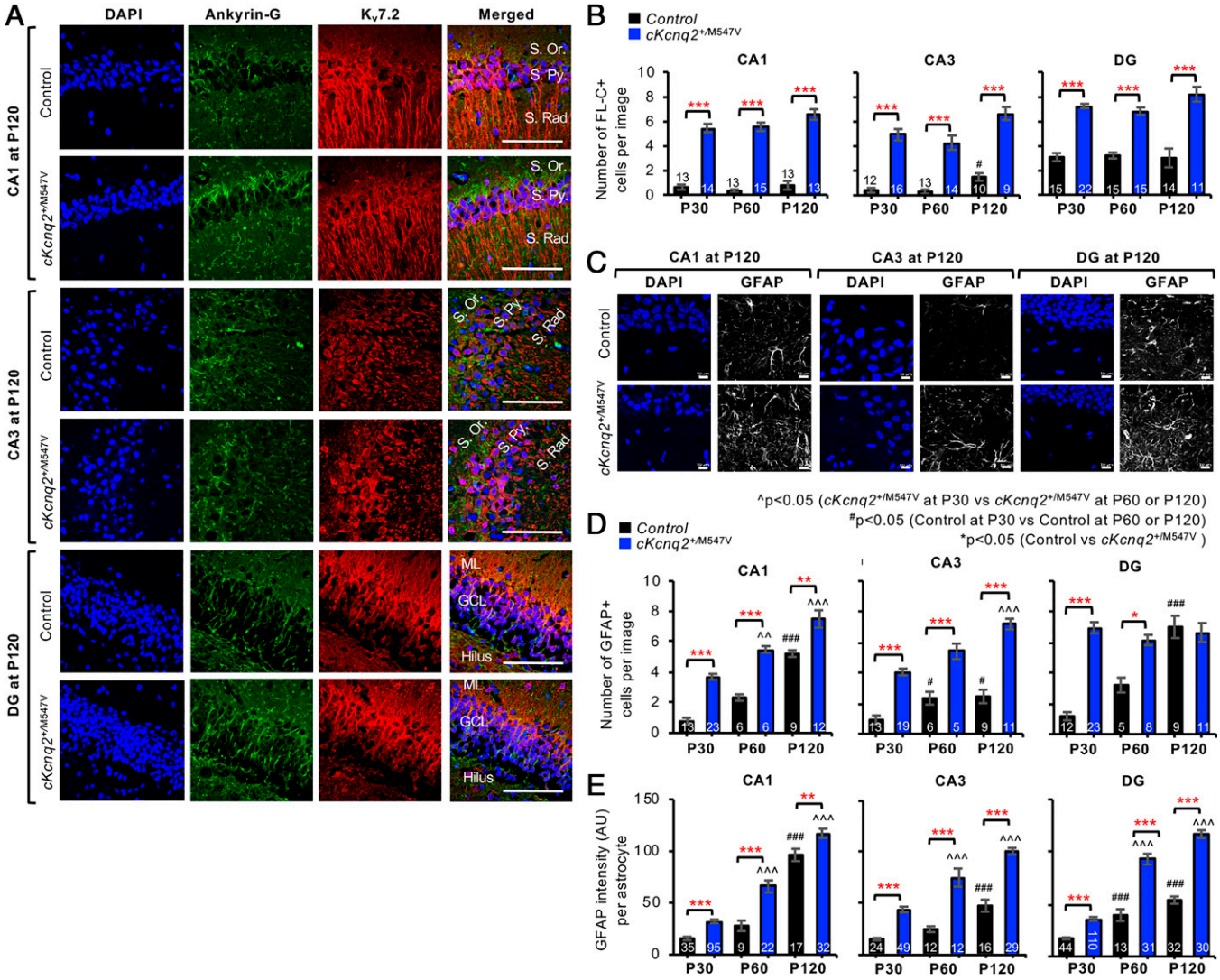

Fig. 4. Conditional *cKcnq2*$^{M547V/+}$ mice displayed neurodegeneration and reactive astrogliosis in their dorsal hippocampi. Coronal brain cryosections of *cKcnq2*$^{+/M547V}$ and control mice (*Kcnq2*-M547V$^{fl/+}$) at P120 were subjected to immunostaining for K_v7.2, ankyrin-G (*A*), EGFP, and GFAP (astrocyte marker) (*C*–*E*), or Fluoro-Jade C (FL-C) staining (*B*). Sections were counterstained with DAPI (nuclear marker). (*A*) Representative fluorescence images of K_v7.2, ankyrin-G, and DAPI in the hippocampal CA1 region. (Scale bars, 100 μm.) Hippocampal pyramidal cell layers: stratum pyramidale (S. Py.), stratum oriens (S. Or.), and stratum radiatum (S. Rad.). Dentate gyrus (DG) cell layers: granule cell layer (GCL), molecular layer (ML), and hilus. (*B*) Quantification of the number of FL-C–positive degenerating neurons in the hippocampi of control and *cKcnq2*$^{+/M547V}$ mice within the image size (160.04 × 160.04 μm). The numbers of images analyzed are indicated in the bar graphs. The number of mice used: $n = 1$ female mouse per genotype at P30 and P60; and $n = 2$ female mice per genotype at P120. Representative images of FL-C staining are shown in *SI Appendix*, Fig. S14. (*C*) Representative fluorescence images of EGFP, GFAP, and DAPI in the hippocampi of control and *cKcnq2*$^{+/M547V}$ mice. (Scale bars, 10 μm.) (*D*) Quantification of the number of GFAP-positive cells within the image size (101.61 × 101.61 μm) of the hippocampi of control and *cKcnq2*$^{+/M547V}$ mice. The numbers of images analyzed are indicated in the bar graphs. (*E*) The mean background-subtracted GFAP fluorescence intensities (arbitrary unit; AU) per GFAP-positive cell in control and *cKcnq2*$^{+/M547V}$ mice. The numbers of GFAP-positive cells analyzed are indicated in the bar graphs. The number of mice and the number of images used are the same as in *D*. Data are shown as mean ± SEM. Post hoc Tukey test results are shown: $^{*}P < 0.05$, $^{**}P < 0.01$, $^{***}P < 0.005$ (control vs. *cKcnq2*$^{+/M547V}$); $^{\#}P < 0.05$, $^{\#\#\#}P < 0.005$ (P30 vs. P60 or P120 in control mice); $^{\wedge\wedge}P < 0.01$, $^{\wedge\wedge\wedge}P < 0.005$ (P30 vs. P60 or P120 in *cKcnq2*$^{+/M547V}$ mice).

Since jumping and rigidity often occur with generalized tonic-clonic convulsions in mouse models of status epilepticus (32), these mice might have displayed subtle behavioral seizures that were not scored by our analyses.

Due to a mild 25 to 40% reduction in current density of heteromeric K_v7 channels, haploinsufficiency is proposed to mediate BFNE caused by *KCNQ2* variants such as A306T and Y284C (31). However, heterozygous KI mice expressing these variants and *Kcnq2*$^{+/-}$ mice do not show spontaneous seizures (19, 21, 33–35). Furthermore, *cKcnq2*$^{+/M547V}$ mice are more susceptible to KA-induced seizures than *Kcnq2*$^{+/-}$ mice (Fig. 2 *D*–*G*). These differences suggest that the seizure phenotypes in *cKcnq2*$^{+/M547V}$ mice do not occur as a simple consequence of the loss of one *KCNQ2* allele.

Although the M546V variant does not reduce current density of heteromeric K_v7.2/K_v7.3 channels in *Xenopus* oocytes (14, 17), it severely decreases axonal surface expression in cultured hippocampal neurons by >70% (14), suggesting that a dominant-negative suppression of axonal K_v7 channels may underlie EE. In support of this idea, a recurrent EE mutation, T274M, in the pore loop exerts a dominant-negative effect by decreasing current density of homomeric channels by 70 to 80% (17) and its heterozygous KI mice develop transient generalized spontaneous seizures from P20 (36). Furthermore,

conditional homozygous deletion of the *Kcnq2* gene from forebrain excitatory pyramidal neurons or genetic suppression of K_v7 current in the first postnatal weeks by overexpressing the $K_v7.2$-containing dominant-negative pore mutation G279S induces spontaneous seizure in mice (11, 37, 38). Thus, we speculate that a significant loss of K_v7 current early in development may contribute to the development of spontaneous seizures in EE.

In *cKcnq2*$^{+/M547V}$ mice, the expression of the *Kcnq2*-M547V-ires-EGFP transgene is driven by the CAG promoter from the Rosa locus in Cre-expressing forebrain glutamatergic neurons, whereas the expression of WT *Kcnq2* is driven by the native promoter (Fig. 1 *B* and *C*), and *Kcnq2* transcript levels are 1.94-fold higher than those in control mice (*SI Appendix*, Fig. S2). This is a different genotype from the human patient containing a heterozygous M546V mutation. The *cKcnq2*$^{+/M547V}$ mice also show the unexpected off-target expression of the transgene in some astrocytes (*SI Appendix*, Fig. S12), although its contribution to seizure and behavioral phenotypes is unclear. However, hippocampal $K_v7.2$ protein levels were comparable between control and *cKcnq2*$^{+/M547V}$ mice at P60 and P120 (Fig. 1*E* and *SI Appendix*, Fig. S4), when seizures and behaviors were examined (Figs. 2 and 3), suggesting that heightened seizure susceptibility and abnormal behaviors are likely due to impaired axonal expression of K_v7 channels.

In *cKcnq2*$^{+/M547V}$ mice born at the expected Mendelian ratio (*SI Appendix*, Fig. S5*C*), we observed postnatal death (Fig. 1*F*), which is considerably earlier than homozygous KI mice of BFNE variants (34) and conditional homozygous $K_v7.2$ KO mice (11). This is relevant to *KCNQ2*-associated EE because most patients appear normal at birth but develop severe seizures and clinical encephalopathy within the first days of life (31). We speculate that neonatal seizures may likely cause the early postnatal death in *cKcnq2*$^{+/M547V}$ mice, as the higher expression of $K_v7.2$-M547V at birth (*SI Appendix*, Fig. S5) is expected to induce forebrain hyperexcitability via its dominant-negative suppression of K_v7 channels. In *KCNQ2*-associated EE, seizure frequency diminishes with age (31). Curiously, *cKcnq2*$^{+/M547V}$ mice that had survived by P21 showed a low risk of mortality (Fig. 1*G*), and displayed reduced $K_v7.2$ expression at P30 (*SI Appendix*, Fig. S3). Although the mechanism underlying this transient decrease in $K_v7.2$ is unknown, our findings suggest that the extent of $K_v7.2$-M547V expression in the early postnatal period may contribute to early mortality.

Effects of the Forebrain Expression of $K_v7.2$-M547V on Cognition and Behavior of Mice. The patient with the M546V mutation had profound intellectual disability and autistic behavior (15). Similarly, *cKcnq2*$^{+/M547V}$ mice display cognitive impairments (Fig. 3). They performed poorly on the OLT (Fig. 3*D*), which tests hippocampus-dependent spatial memory (24). Similar hippocampus-dependent spatial memory deficits were reported in the heterozygous T274M KI mice (36) and transgenic mice overexpressing dominant-negative $K_v7.2$-G279S (37). The *cKcnq2*$^{+/M547V}$ mice also showed deficits in nonspatial memory of object identity in NORT (Fig. 3*D*), which relies on the perirhinal cortex and to a lesser extent the hippocampus (24, 39). Neuronal hyperexcitability and degeneration in the hippocampus and cortex (Figs. 2 and 4 and *SI Appendix*, Figs. S9–S13) may underlie these memory deficits in *cKcnq2*$^{+/M547V}$ mice.

We also observed locomotor hyperactivity of *cKcnq2*$^{+/M547V}$ males (Fig. 3*C*) similar to the transgenic males overexpressing dominant-negative $K_v7.2$-G279S (37). Hippocampal sclerosis in these mice (Fig. 4*C*) (37) may underlie their locomotor hyperactivity given that hippocampal lesion and damage result in heightened locomotion in mice (40). Although the open-field test performed under aversive bright light is widely used to examine anxiety in mice (41), increased entry and duration of *cKcnq2*$^{+/M547V}$ mice to the exposed center in the dark (Fig. 3*C*) suggests their enhanced exploratory behavior in novel environments. Interestingly, the heterozygous T274M KI mice do not exhibit changes in anxiety, exploration, and repetitive behaviors (36). These behavioral differences suggest that the M546V mutation may have a different pathophysiology from the T274M mutation.

Comparison between *cKcnq2*$^{+/M547V}$ and *Kcnq2*$^{+/-}$ mice revealed that both genotypes show enhanced repetitive behaviors (Fig. 3 *F* and *G*) (22), which is one of the core clinical symptoms of autism (42). Since *cKcnq2*$^{+/M547V}$ mice have heterozygous forebrain expression of $K_v7.2$-M547V in *Kcnq2*$^{+/-}$ mice (Fig. 1*B*) and repetitive grooming behavior is mediated by GABAergic output from the striatum (43), we speculate that enhanced repetitive behaviors in *cKcnq2*$^{+/M547V}$ mice may likely be due to the heterozygous loss of *Kcnq2* in the striatum. In the three-chamber social interaction test, only *cKcnq2*$^{+/M547V}$ females showed a mild reduction in sociability (Fig. 3*E*), which might be contributed by the hyperactivity and damage in the hippocampus and cortex (Figs. 2 and 4 and *SI Appendix*, Figs. S9–S13), important for social approach and cognition (44, 45).

Neuropathology in Mouse Forebrain Induced by $K_v7.2$-M547V. The present study provides evidence that the expression of EE mutant $K_v7.2$-M547V induces neurodegeneration and reactive astrogliosis in the hippocampus and cortex of mice (Fig. 4). These findings are consistent with the MRI of a patient with the M546V mutation, which showed substantial brain lesions and neuronal loss indicated by small frontal lobes, thinned splenium of the corpus callosum, ventriculomegaly, and increased cerebral spinal fluid space (15). This patient also showed intractable seizures (15). In mesial temporal lobe epilepsy, hippocampal sclerosis is closely associated with drug-resistant seizures, progressive cognitive decline, high risk of mortality, and sudden unexpected death in epilepsy (46). Although epileptic seizures are thought to cause cognitive and behavioral impairments in EE (1, 47), our findings suggest that severe seizure phenotypes, reduced viability, and cognitive deficits seen in *cKcnq2*$^{+/M547V}$ mice may be due to neurodegeneration and neuroinflammation in addition to hyperexcitability in the hippocampus and cortex (Figs. 2–4 and *SI Appendix*, Figs. S9–S14).

It is noteworthy that neurodegeneration and neuroinflammation were observed in *cKcnq2*$^{+/M547V}$ mice and mice overexpressing $K_v7.2$-G279S but not in mice heterozygous for $K_v7.2$-T274M, even though all three mutations cause dominant-negative suppression of K_v7 channels (36–38). These differences may be related to transgene promoter effects in vivo (exogenous promoter vs. native promoter) and different "mutant over WT" expression ratios, which dictate the extent of dominant-negative suppression of tetrameric K^+ channels (48). However, these differences also highlight the complexity and heterogeneity of the pathophysiology associated with each mutation. Whereas the T274M mutation induces dominant-negative current suppression of human $K_v7.2$ channels (17), the analogous mutation to M547V in the human $K_v7.2$ short isoform (M518V) not only blocks their current and protein expression by increasing ubiquitination but also induces dominant-negative suppression of axonal K_v7 channels by retaining them intracellularly (14). These unique effects on $K_v7.2$ expression may contribute to neurodegeneration.

It is unclear how expression of $K_v7.2$-M547V results in neurodegeneration in vivo. The M547V-induced severe reduction in axonal K_v7 channels in the forebrain excitatory neurons and subsequent increase in their excitability may lead to excitotoxicity induced by excessive release of glutamate. The same mutation is also expected to induce ubiquitination and proteasome degradation of $K_v7.2$, whereas the presence of $K_v7.3$ blocks this degradation and induces intracellular accumulation of ubiquitinated $K_v7.2$ (14). Since impairment of the ubiquitin-

proteasome system and ER stress response can activate programmed cell death (28), we speculate that intracellular retention of $K_v7.2$-M547V proteins in the ER and their continuous clearance could saturate the capacity of the ER and proteasome, leading to apoptosis. Future studies shall test these hypotheses to identify the mechanisms underlying neurodegeneration and its contribution to refractory seizures associated with this EE variant.

Materials and Methods

Generation of Conditional Forebrain Heterozygous KI of $K_v7.2$-M547V in Mice. The transgenic mice for conditional expression of the mouse *Kcnq2* gene containing the M547V mutation (ATG to GTG) (designated as *Kcnq2*-M547V$^{fl/+}$) on the C57BL/6J genetic background were generated at Cyagen Biosciences by CRISPR-Cas–mediated genome engineering (49). In these mice, the cassette CAG-LoxP-Stop-LoxP-*Kcnq2-M547V-IRES-EGFP*-polyA was cloned into intron 1 of the Gt(ROSA)26Sor locus on mouse chromosome 6 (GenBank accession no. NR_027008.1) in a reverse direction. This cassette was flanked by 2.5- and 4.5-kb homology arms, which were generated by PCR using a bacterial artificial chromosome (BAC) clone from the C57BL/6J library as template. To induce heterozygous expression of *Kcnq2-M547V-IRES-EGFP* in the forebrain pyramidal neurons via Cre-mediated removal of an upstream floxed-STOP cassette (designated as *cKcnq2*$^{+/M547V}$ mice), *Kcnq2*-M547V$^{fl/fl}$ mice were crossed to heterozygous *Kcnq2* KO *Kcnq2*$^{tm1Dgen/+}$ mice (designated as *Kcnq2*$^{+/-}$; Jax.org stock 005830) and Emx1$^{cre/cre}$ mice (Jax.org stock 005628). Both *Kcnq2*$^{tm1Dgen/+}$ and Emx1$^{cre/cre}$ mice were in the C57BL/6J background (19, 20). The control mice used in these studies were *Kcnq2*$^{+/+}$, *Kcnq2*-M547V$^{fl/+}$, *Kcnq2*-M547V$^{fl/fl}$, Emx1$^{cre/+}$, and Emx1$^{cre/cre}$ mice.

Video-ECoG Monitoring in Freely Moving Mice. To examine spontaneous seizures, mice at P51 to P108 were subjected to a video EEG monitoring system (Pinnacle Technology) from 2:00 to 4:30 PM as described (50). The electrical signal was band pass–filtered from 1 to 100 Hz and digitized at 200 Hz. EEG epileptiform activity was identified by repetitive occurrence, large amplitude, and sharp morphology compared with baseline EEG activity (50).

Kainate-Induced Seizures. Behavioral seizures were induced in mice (P120 to P180) with KA (15 mg/kg, i.p.; Abcam) and monitored using a modified Racine, Pinal, and Rovner scale as described (22).

Behavioral Studies. Behavioral tests with a test interval of >2 d were started at P120 as described (22) from least to most invasive assays in the following order: object location and novel object recognition, self-grooming, marble burying, open field, rotarod, and three-chamber social interaction tests.

Immunohistochemistry of Mouse Brain Cryosections. Coronal brain cryosections (20-μm-thick) were immunostained with antibodies for $K_v7.2$ (Synaptic Systems), ankyrin-G, GFAP (NeuroMab), and GFP (Abcam) or stained for Fluoro-Jade C (Biosensis) and DAPI (Invitrogen) after permeabilization. Confocal fluorescent images (1-μm optical distance) were analyzed by the ImageJ program (NIH) and our algorithm "ANIMA."

Statistical Analysis. Data are reported as mean ± SEM. OriginPro v9.5 (OriginLab) was used to perform statistical analyses. Comparisons between two groups were conducted with the Student's two-tailed *t* test. Behavioral data were also analyzed using two-way ANOVA. Tukey tests were used to establish post hoc pairwise differences between means. A P value < 0.05 was considered statistically significant.

A detailed description of each method is provided in *SI Appendix*.

Data Availability. All study data are included in the article and/or supporting information. The source data sets that were generated and analyzed during the current study and presented as main Figures and supplementary figures are available in the Figshare repository (DOI: 10.6084/m9.figshare.17124350).

ACKNOWLEDGMENTS. This research was supported by the NIH under Awards R01 NS083402, R01 NS100019, and R01 NS097610 (to H.J.C.) and R01 NS105825 and R03 NS103029 (to C.A.C.-H.), and R21 NS104293 and R21 NS109894 (to J.S.R.) from the National Institute of Neurological Disorders and Stroke.

1. A. T. Berg *et al.*, Revised terminology and concepts for organization of seizures and epilepsies: Report of the ILAE Commission on Classification and Terminology, 2005–2009. *Epilepsia* **51**, 676–685 (2010).
2. A. McTague, K. B. Howell, J. H. Cross, M. A. Kurian, I. E. Scheffer, The genetic landscape of the epileptic encephalopathies of infancy and childhood. *Lancet Neurol.* **15**, 304–316 (2016).
3. EpiPM Consortium, A roadmap for precision medicine in the epilepsies. *Lancet Neurol.* **14**, 1219–1228 (2015).
4. A. S. Allen *et al.*, Epi4K Consortium; Epilepsy Phenome/Genome Project, De novo mutations in epileptic encephalopathies. *Nature* **501**, 217–221 (2013).
5. J. Noebels, Pathway-driven discovery of epilepsy genes. *Nat. Neurosci.* **18**, 344–350 (2015).
6. D. A. Brown, G. M. Passmore, Neural KCNQ (Kv7) channels. *Br. J. Pharmacol.* **156**, 1185–1195 (2009).
7. Z. Pan *et al.*, A common ankyrin-G-based mechanism retains KCNQ and NaV channels at electrically active domains of the axon. *J. Neurosci.* **26**, 2599–2613 (2006).
8. H. J. Chung, Y. N. Jan, L. Y. Jan, Polarized axonal surface expression of neuronal KCNQ channels is mediated by multiple signals in the KCNQ2 and KCNQ3 C-terminal domains. *Proc. Natl. Acad. Sci. U.S.A.* **103**, 8870–8875 (2006).
9. V. Bennett, D. N. Lorenzo, An adaptable spectrin/ankyrin-based mechanism for long-range organization of plasma membranes in vertebrate tissues. *Curr. Top. Membr.* **77**, 143–184 (2016).
10. M. M. Shah, M. Migliore, I. Valencia, E. C. Cooper, D. A. Brown, Functional significance of axonal Kv7 channels in hippocampal pyramidal neurons. *Proc. Natl. Acad. Sci. U.S.A.* **105**, 7869–7874 (2008).
11. H. Soh, R. Pant, J. J. LoTurco, A. V. Tzingounis, Conditional deletions of epilepsy-associated KCNQ2 and KCNQ3 channels from cerebral cortex cause differential effects on neuronal excitability. *J. Neurosci.* **34**, 5311–5321 (2014).
12. D. L. Greene, N. Hoshi, Modulation of Kv7 channels and excitability in the brain. *Cell. Mol. Life Sci.* **74**, 495–508 (2017).
13. J. Zhang *et al.*, Identifying mutation hotspots reveals pathogenetic mechanisms of KCNQ2 epileptic encephalopathy. *Sci. Rep.* **10**, 4756 (2020).
14. E. C. Kim *et al.*, Reduced axonal surface expression and phosphoinositide sensitivity in K_v7 channels disrupts their function to inhibit neuronal excitability in Kcnq2 epileptic encephalopathy. *Neurobiol. Dis.* **118**, 76–93 (2018).
15. S. Weckhuysen *et al.*, KCNQ2 encephalopathy: Emerging phenotype of a neonatal epileptic encephalopathy. *Ann. Neurol.* **71**, 15–25 (2012).
16. J. J. Millichap *et al.*, KCNQ2 encephalopathy: Features, mutational hot spots, and ezogabine treatment of 11 patients. *Neurol. Genet.* **2**, e96 (2016).
17. G. Orhan *et al.*, Dominant-negative effects of KCNQ2 mutations are associated with epileptic encephalopathy. *Ann. Neurol.* **75**, 382–394 (2014).
18. J. P. Cavaretta *et al.*, Polarized axonal surface expression of neuronal KCNQ potassium channels is regulated by calmodulin interaction with KCNQ2 subunit. *PLoS One* **9**, e103655 (2014).
19. A. V. Tzingounis, R. A. Nicoll, Contribution of KCNQ2 and KCNQ3 to the medium and slow afterhyperpolarization currents. *Proc. Natl. Acad. Sci. U.S.A.* **105**, 19974–19979 (2008).
20. J. A. Gorski *et al.*, Cortical excitatory neurons and glia, but not GABAergic neurons, are produced in the Emx1-expressing lineage. *J. Neurosci.* **22**, 6309–6314 (2002).
21. H. Watanabe *et al.*, Disruption of the epilepsy KCNQ2 gene results in neural hyperexcitability. *J. Neurochem.* **75**, 28–33 (2000).
22. E. C. Kim *et al.*, Heterozygous loss of epilepsy gene KCNQ2 alters social, repetitive and exploratory behaviors. *Genes Brain Behav.* **19**, e12599 (2020).
23. Y. Ben-Ari, R. Cossart, Kainate, a double agent that generates seizures: Two decades of progress. *Trends Neurosci.* **23**, 580–587 (2000).
24. J. K. Denninger, B. M. Smith, E. D. Kirby, Novel object recognition and object location behavioral testing in mice on a budget. *J. Vis. Exp.* **141**, e58593 (2018).
25. S. S. Moy *et al.*, Sociability and preference for social novelty in five inbred strains: An approach to assess autistic-like behavior in mice. *Genes Brain Behav.* **3**, 287–302 (2004).
26. J. L. Silverman, M. Yang, C. Lord, J. N. Crawley, Behavioural phenotyping assays for mouse models of autism. *Nat. Rev. Neurosci.* **11**, 490–502 (2010).
27. M. Angoa-Pérez, M. J. Kane, D. I. Briggs, D. M. Francescutti, D. M. Kuhn, Marble burying and nestlet shredding as tests of repetitive, compulsive-like behaviors in mice. *J. Vis. Exp.* **82**, 50978 (2013).
28. J. Tyedmers, A. Mogk, B. Bukau, Cellular strategies for controlling protein aggregation. *Nat. Rev. Mol. Cell Biol.* **11**, 777–788 (2010).
29. L. C. Schmued, C. C. Stowers, A. C. Scallet, L. Xu, Fluoro-Jade C results in ultra high resolution and contrast labeling of degenerating neurons. *Brain Res.* **1035**, 24–31 (2005).
30. S. A. Liddelow, B. A. Barres, Reactive astrocytes: Production, function, and therapeutic potential. *Immunity* **46**, 957–967 (2017).
31. F. Miceli *et al.*, "KCNQ2-related disorders" in *GeneReviews®*, M. P. Adam *et al.*, Eds. (University of Washington, Seattle, WA, 2010; updated 2018). https://www.ncbi.nlm.nih.gov/books/NBK32534/.
32. S. Sharma, S. Puttachary, A. Thippeswamy, A. G. Kanthasamy, T. Thippeswamy, Status epilepticus: Behavioral and electroencephalography seizure correlates in kainate experimental models. *Front. Neurol.* **9**, 7 (2018).
33. J. F. Otto *et al.*, Electroconvulsive seizure thresholds and kindling acquisition rates are altered in mouse models of human KCNQ2 and KCNQ3 mutations for benign familial neonatal convulsions. *Epilepsia* **50**, 1752–1759 (2009).

34. N. A. Singh *et al.*, Mouse models of human KCNQ2 and KCNQ3 mutations for benign familial neonatal convulsions show seizures and neuronal plasticity without synaptic reorganization. *J. Physiol.* **586**, 3405–3423 (2008).
35. Y. Tomonoh *et al.*, The kick-in system: A novel rapid knock-in strategy. *PLoS One* **9**, e88549 (2014).
36. M. Milh *et al.*, A knock-in mouse model for KCNQ2-related epileptic encephalopathy displays spontaneous generalized seizures and cognitive impairment. *Epilepsia* **61**, 868–878 (2020).
37. H. C. Peters, H. Hu, O. Pongs, J. F. Storm, D. Isbrandt, Conditional transgenic suppression of M channels in mouse brain reveals functions in neuronal excitability, resonance and behavior. *Nat. Neurosci.* **8**, 51–60 (2005).
38. S. L. Marguet *et al.*, Treatment during a vulnerable developmental period rescues a genetic epilepsy. *Nat. Med.* **21**, 1436–1444 (2015).
39. E. C. Warburton, M. W. Brown, Neural circuitry for rat recognition memory. *Behav. Brain Res.* **285**, 131–139 (2015).
40. S. M. Thompson, L. E. Berkowitz, B. J. Clark, Behavioral and neural subsystems of rodent exploration. *Learn. Motiv.* **61**, 3–15 (2018).
41. K. R. Bailey, J. N. Crawley, "Anxiety-related behaviors in mice" in *Methods of Behavioral Analysis in Neuroscience*, J. J. Buccafusco, Ed. (CRC Press/Routledge/Taylor & Francis Group, Boca Raton, FL, 2009), pp. 77–101.
42. J. A. S. Vorstman *et al.*, Autism genetics: Opportunities and challenges for clinical translation. *Nat. Rev. Genet.* **18**, 362–376 (2017).
43. K. Zhang, K. Hill, S. Labak, G. J. Blatt, J. J. Soghomonian, Loss of glutamic acid decarboxylase (Gad67) in Gpr88-expressing neurons induces learning and social behavior deficits in mice. *Neuroscience* **275**, 238–247 (2014).
44. T. Okuyama, T. Kitamura, D. S. Roy, S. Itohara, S. Tonegawa, Ventral CA1 neurons store social memory. *Science* **353**, 1536–1541 (2016).
45. M. Murugan *et al.*, Combined social and spatial coding in a descending projection from the prefrontal cortex. *Cell* **171**, 1663–1677.e16 (2017).
46. K. Malmgren, M. Thom, Hippocampal sclerosis—Origins and imaging. *Epilepsia* **53** (suppl. 4), 19–33 (2012).
47. B. Hermann, M. Seidenberg, Epilepsy and cognition. *Epilepsy Curr.* **7**, 1–6 (2007).
48. N. A. Minassian, M. C. Lin, D. M. Papazian, Altered Kv3.3 channel gating in early-onset spinocerebellar ataxia type 13. *J. Physiol.* **590**, 1599–1614 (2012).
49. B. Hall *et al.*, Genome editing in mice using CRISPR/Cas9 technology. *Curr. Protoc. Cell Biol.* **81**, e57 (2018).
50. M. L. Casalia, M. A. Howard, S. C. Baraban, Persistent seizure control in epileptic mice transplanted with gamma-aminobutyric acid progenitors. *Ann. Neurol.* **82**, 530–542 (2017).